Hindawi
Bioinorganic Chemistry and Applications
Volume 2021, Article ID 6209094, 8 pages
https://doi.org/10.1155/2021/6209094

Research Article

Feasibility of Using H_3PO_4/H_2O_2 in the Synthesis of Antimicrobial TiO_2 Nanoporous Surfaces

Benjamín Valdez-Salas and Ernesto Beltrán-Partida

Departamento de Corrosión y Materiales Avanzados, Instituto de Ingeniería, Universidad Autónoma de Baja California, Blvd. Benito Juárez y Calle de la Nomal S/N, Mexicali B.C. 21040, Mexico

Correspondence should be addressed to Benjamín Valdez-Salas; benval@uabc.edu.mx and Ernesto Beltrán-Partida; beltrane@uabc.edu.mx

Received 18 September 2021; Revised 17 November 2021; Accepted 26 November 2021; Published 11 December 2021

Academic Editor: Giuseppe Ciccarella

Ti6Al4V alloys are the primary materials used for clinical bone regeneration and restoration; however, they are substantially susceptible to biomaterial-related infections. Therefore, in the present work, we applied a controllable and stable oxidative nanopatterning strategy by applying H_3PO_4, a weaker dissociating acid, as a substitute for H_2SO_4 in the classical piranha reaction. The results suggest that our method acted as a concomitant platform to develop reproducible diameter-controlled TiO_2 nanopores (NPs). Interestingly, our procedure illustrated stable temperature reactions without exothermic responses since the addition of mixture preparation to the nanopatterning reactions. The reactions were carried out for 30 min (NP14), 1 h (NP7), and 2 h (NP36), suggesting the formation of a thin nanopore layer as observed by Raman spectroscopy. Moreover, the antimicrobial activity revealed that NP7 could disrupt active microbial colonization for 2 h and 6 h. The phenotype configuration strikingly showed that NP7 does not alter the cell morphology, thus proposing a disruptive adhesion pathway instead of cellular lysis. Furthermore, preliminary assays suggested an early promoted osteoblasts viability in comparison to the control material. Our work opens a new path for the rationale design of nanobiomaterials with "intelligent surfaces" capable of decreasing microbial adhesion, increasing osteoblast viability, and being scalable for industrial transfer.

1. Introduction

Titanium (Ti) and its alloy (Ti6Al4V) are the main biocompatible metallic options currently used to promote bone formation and restoration [1]. However, contamination by microbial adhesion can negatively compromise Ti effectiveness and clinical success. Promising strategies have been reported to generate nanopatterned surfaces to control microbial adhesion. For example, roughness in texture, deposition of antimicrobial nanocoatings, and nanoscale tuned surfaces [2, 3]. Of particular interest, the fabrication of controlled-sized TiO_2 NPs has emerged as a current trend for controlling microbial adhesion and colonization [4]. Interestingly, chemical oxidative nanopatterning has proven to be a versatile strategy for the development of controlled NP tuned surfaces [5]. Thus far, the H_2SO_4/H_2O_2 system (piranha solution) is the optimal etching/oxidative protocol for the generation of reproducible NPs and the activation of metallic surfaces. Nonetheless, the mixture with strong acids exacerbates an extreme exothermic reaction that acts violently after organic matter contact (at low concentrations) and on metallic surfaces [6]. Consequently, it is substantial to develop a stable and nonexothermic etching solution for chemical nanopatterning capable of producing NPs on Ti6Al4V surfaces. Thus, by applying H_3PO_4, a weaker dissociation acid of pKa lower than H_2SO_4 [7, 8], we could reduce the exothermic reactivity on Ti6Al4V without disturbing the formation of reproducible NPs.

Therefore, our work aims to synthesize diameter-controlled and reproducible NPs on Ti6Al4V to reduce microbial adhesion and promote early osteoblast growth using an oxidative nanopatterning procedure with H_3PO_4/H_2O_2. This

strategy is an excellent alternative to the piranha solution since it is more stable, ecofriendly, and nonexothermic suspension without requiring heating conditions.

2. Materials and Methods

2.1. Synthesis and Characterization of NPs. Ti6Al4V foils (ASTM F136) with 10.0 mm^2 and 1 mm thickness were polished with SiC emery paper following 1-μm alumina and ultrasonically cleaned for 30 min in absolute ethanol. The NPs were synthesized using a formulation of 85% H_3PO_4 and 30% H_2O_2 (Sigma-Aldrich, USA) in a 1 : 1 volume ratio at room temperature (RT) for 30 (NP14), 60 (NP7), and 120 min (NP36), to fabricate different diameters. Afterward, the materials were cleaned in ultrapure water for 15 min under sonication, rinsed with ethyl alcohol, and dried before each analysis. The experimental materials were sterilized in a biosecurity cabinet using UV irradiation (285 nm UVB light source) for 30 min each side. Cleaned and sterilized Ti6Al4V foils without any chemical treatment were used as controls for the experimental testing.

2.2. Surface Physicochemical Characterization. The surface morphology was analyzed using field-emission scanning electron microscopy (FE-SEM; Tescan LYRA 3) at a 20 kV accelerating voltage with a secondary electron detector. The NP distribution was generated from 50 NPs randomly measured from a FE-SEM micrograph. Energy dispersive X-ray spectroscopy (EDX, Brucker XFlash) coupled to the FE-SEM was used for the chemical analysis. Raman spectroscopy (Raman Station 400F Perkin-Elmer) was applied at RT using a 785 nm diode laser beam at a power of 15 mW. The water contact angle (WCA) was quantified using an automated tensiometer (Theta Attension; Biolin Scientific), placing a 5 μL droplet of deionized water at RT and 45% relative humidity.

2.3. Microbial Characterization. We prepared fresh overnight grown cultures of *Staphylococcus aureus* (*S. aureus*, ATCC 25923), *Escherichia coli* (*E. coli*, ATCC 25922), and an isolated *C. albicans* strain as previously described [9]. The active fungal suspension was adjusted to 2×10^4 CFU/mL with Sabouraud dextrose (SD) broth. Then, 50 μL of the working *C. albicans* were cultured over the surfaces, which were individually placed in a 12-well plate (Corning, USA). Similarly, the *S. aureus* and *E. coli* inoculums were tailored to 1×10^7 CFU/mL using tryptic soy (TS) broth and cultured. The materials were incubated for 2 h and 6 h (defined as initial and late adhesion, respectively) at 37°C in static conditions, washed thrice with 1 × phosphate-buffered saline (PBS) for 5 min and ultrasonicated in 2 mL of SD or TS broth [10]. The remaining suspensions were serially diluted and cultured in SD (*C. albicans*) or TS (bacterial cells) agar for 24 h at 37°C.

2.4. FE-SEM Microbial Analysis. For FE-SEM analysis, each material was rinsed thrice with warm PBS, fixed in 3% glutaraldehyde (Sigma-Aldrich, USA) at 4°C overnight, rinsed thrice with PBS, and postfixed with 3% glutaraldehyde for 2 h at RT. The samples were dehydrated in a graded series of ethanol for 2 h and placed into a desiccator until the analysis.

2.5. Cytotoxicity Assessment Using MTT. In order to analyze the cytotoxicity of the experimental surfaces, we applied the MTT (3-(4,5-dimethylthiazol-2-yl)-2,5-diphenyltetrazolium bromide) viability assay [11]. We used MG-63 human osteoblast-like cells (ATCC CRL-1427). Prior to cell culture, each experimental material was placed in an individual well of a 12-well polystyrene plate (Corning, USA). The initial cell density was 1×10^4 cells/surface in passage three. They were harvested and cultured in complete medium constituted of Dulbecco's modified Eagle's medium (DMEM, Thermo Fisher Scientific, USA) supplemented with 10% heat-inactivated fetal bovine serum (Thermo Fisher Scientific, USA) and 100 units/mL of penicillin-streptomycin (Thermo Fisher Scientific, USA) at 37°C in a humidified 5% CO_2 incubator for 24 h. Afterward, the cells were washed thrice with warm PBS. 2 mL of MTT (Sigma-Aldrich, USA) in DMEM (5 mg/mL) was added into each well and further incubated at 37°C in a humidified 5% CO_2 incubator for 3 h. The resulting formazan crystals were dissolved after discarding the medium containing MTT and transferring the 12-well plate into an orbital shaker at 200 rpm, 37°C with dimethyl sulfoxide (Sigma-Aldrich, USA) for 20 min. Then, the dissolved crystals were deposited into a 96-well polystyrene plate (Sigma-Aldrich, USA), and the optical density (O.D.) was recorded at 590 nm using a microplate reader (Thermoskan, Thermo Fisher Scientific, USA).

2.6. Statistical Analysis. Numerical data of three independent studies performed each in triplicate were assessed by one-way analysis of variance followed by Tukey's multiple comparison test using GraphPad Prism 7. A $P < 0.05$ was considered statistically significant.

3. Results and Discussion

Figure 1(a) illustrates diameter-controlled NPs on Ti6Al4V surfaces after the nanopatterning protocol. Moreover, the high-zoom revealed the formation of homogeneous and ordered nanostructures for each reaction. Figure 1(b) represents NPs of ≈7 nm (1 h), ≈14 nm (30 min), and ≈36 nm (2 h), indicating that time could be the predominant thermodynamic parameter for NP diameter control at room temperature using the H_3PO_4 system. The EDX showed the materials' elemental values (Figure 1(c)), highlighting that phosphorous (P) was not incorporated as a doping complexing element in any treatment. However, EDX is a technology that enables chemical profiling of the X-ray photons generated from the beamed electrons of the deeper layers of the surface [12]. The X-ray photoelectron spectroscopy (XPS) is recommended for clarifying this interesting trend. It is important to note that phosphate coatings could generate electrostatic interactions that might be favorable for promoting bacterial adhesion [13]. Furthermore, the low carbon levels suggest the absence of any organic pollutants

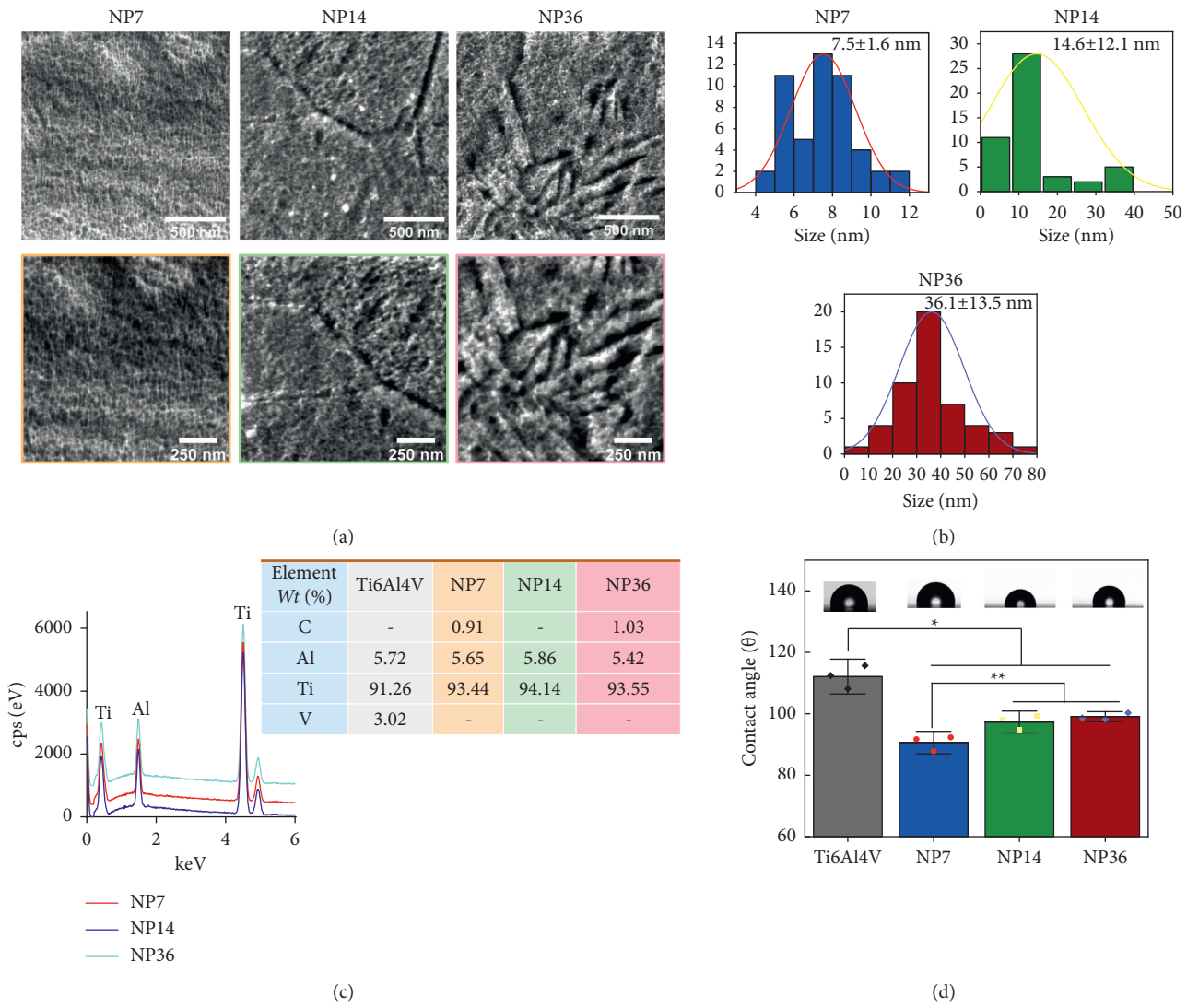

Figure 1: (a) FE-SEM of the synthesized materials. (b) Diameter distribution of the NPs. (c) EDX of the surfaces. (d) WCA of the specimens. The symbols * and ** show significant differences between the materials.

(Figure 1(c)). Thus, the lower carbon level and the nanostructured distribution detected on the NPs, especially on NP7, could be attributed to the reduced WCA (Figure 1(d)). The reactions achieved Ti^{4+} by an initial oxidation, followed by the dissolution of the oxide layer, and the nucleation of a thin oxide layer. Thus, decomposing H_2O_2 into O_2 and H^+ generates nanodefects [14].

$$\begin{aligned} 2H_2O_2 &\longrightarrow 2H_2O + O_2 \\ Ti + 2H_2O_2 + 4H^+ &\longrightarrow Ti^{4+} + 4H_2O \\ Ti + 4H^+ &\longrightarrow Ti^{4+} + 2H_2 \\ Ti + O_2 + 2H_2O &\longrightarrow Ti^{4+} + 4OH^-. \end{aligned} \quad (1)$$

The enlarged atomic vacancies increased the pores, surface area, and free energy of samples. Furthermore, Ti^{4+} generates unstable cationic complexes $[Ti_2O_5(OH)_2]^+$, $[Ti_2O_5(OH)_2]$, and $[Ti_2O_5(OH)_4]^+$ that decompose into $(Ti(OH)_4)$ [15]. In a previous study, Pisarek et al. suggested that H_3PO_4/H_2O_2 at RT after 24 h conducted to form a nanosponge-like surface morphology [16]. Similarly, the authors detected the presence of Ti $2p_{3/2}$ and O1 s signals that have been ascribed for the Ti-O bond gap, thus proposing the formation of a consistent thick layer mainly of TiO_2. Interestingly, the Raman analysis (Figure 2) suggests that a thinner TiO_2 layer could be generated after the nanopatterning process, as there was no bandgap between 800 and 200 nm corresponding to amorphous TiO_2 [17, 18]. Although the presence of NPs was detected for all the experimental materials, the EDX results also supported this interesting finding, as no oxygen levels were detected. More surface chemistry analyses are recommended in order to support those interesting findings. On the other hand, the study by Pisarek reported that the 24 h treatment phase resulted in the deposition of phosphate ions [16], and far more critical is the fact of possible corrosion detriments by the extensive reaction period. Although this oxidative strategy was applied in previous studies, the role of

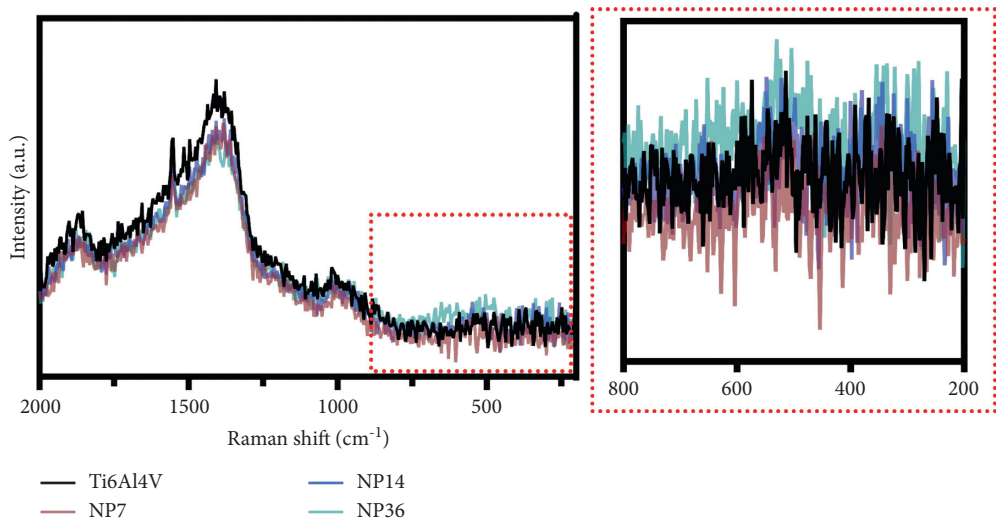

Figure 2: Raman characterization of the experimental materials.

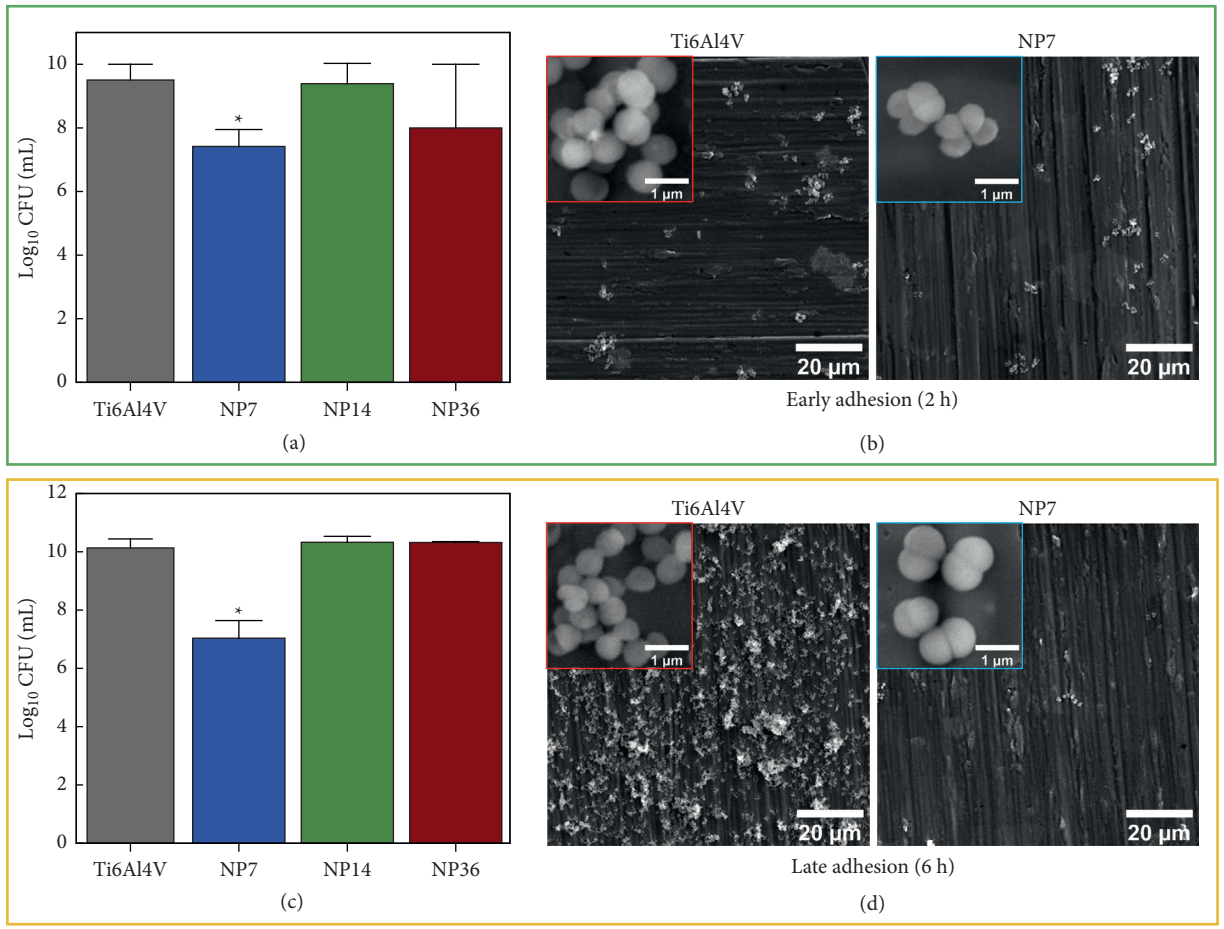

Figure 3: Antibacterial behavior on the experimental materials. (a) Bacterial viability after 2 h of incubation. (b) *S. aureus* morphology on the control and NP7 material at early adhesion phase. (c) *S. aureus* growing viability after 6 h. (d) *S. aureus* phenotype characterization at the late adhesion. The symbol * shows significant cell viable differences between the material groups.

treatment time for NPs diameter variations was not examined. Previously, Variola et al. synthesized NPs on Ti6Al4V using the piranha solution at RT, interestingly, under extreme caution [1]. The authors showed NP diameters comparable to those of NP7 and NP14. However, the opposite effect was detected in NP36, probably by

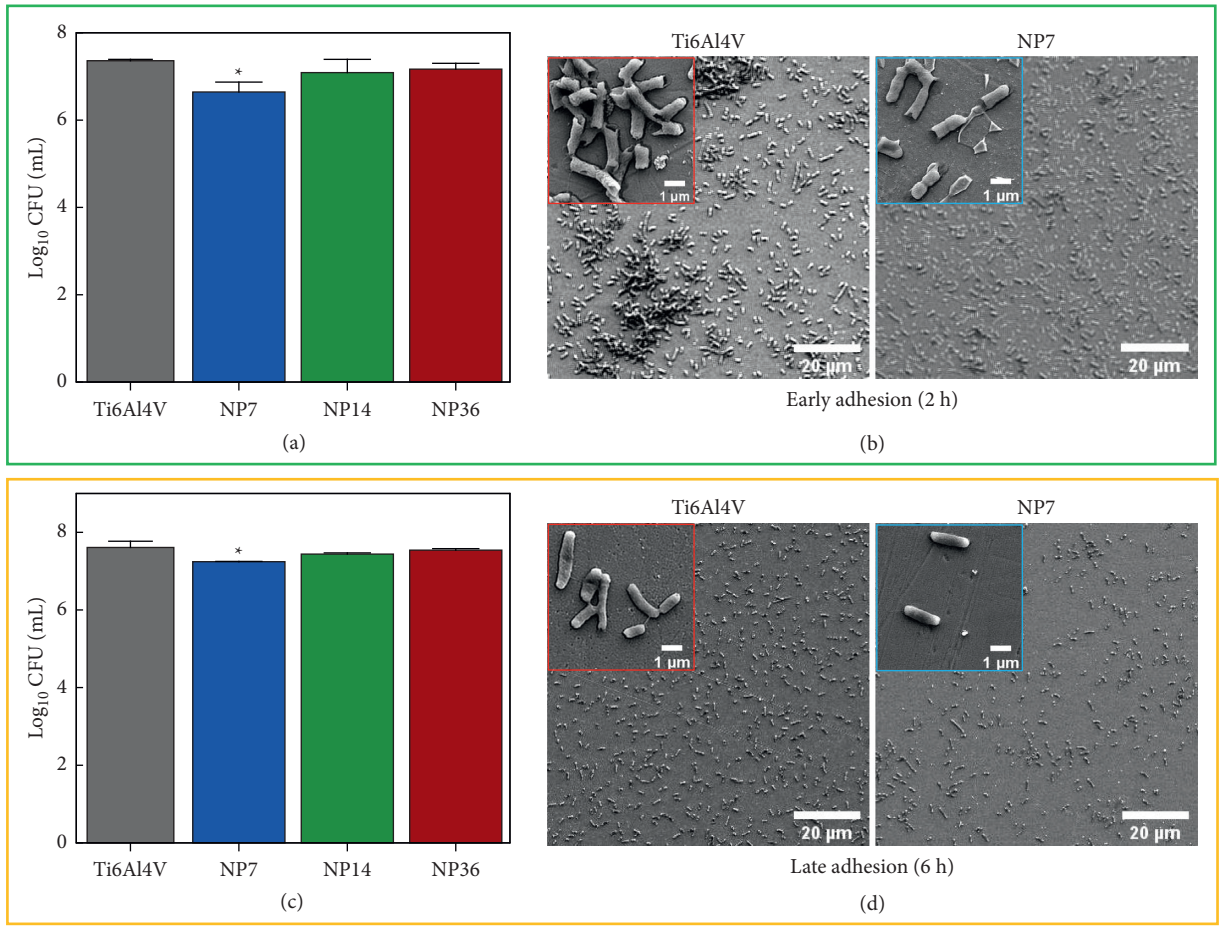

Figure 4: Antibacterial behavior of *E. coli* on the experimental materials. (a) Viability evaluation after 2 h of incubation. (b) *E. coli* morphology on the control and NP7 material at early adhesion phase. (c) *E. coli* growing viability after 6 h. (d) *E. coli* phenotype characterization at the late adhesion. The symbol * shows significant cell viable differences between the material groups.

generating new single nanocavities and pits growing together increasing the diameter. Moreover, it has been described that oxidative etching procedures favor the attack of *ß*-grains over the *α*-grains, therefore altering the surface microtexture over time [1, 19]. Nonetheless, those discrepancies could not be comprehensively harbored in the nanopatterning onsets. Further it is considered that the chemical nature of the acids (H_3PO_4 versus H_2SO_4) can influence the kinetics and thermodynamics of the reactions. This phenomenon could have been due to the application of a weaker acid such as H_3PO_4, which may demand prolonged etching periods as compared to H_2SO_4. Correspondingly, this result is in accordance with the thin nanostructured coatings generated on Ti6Al4V using weaker acids/oxidants that also require extreme care protocols [5]. On the contrary, the H_3PO_4/H_2O_2 system showed hallmarked constant temperature stability beginning from the mixture preparation to each performed reaction. Therefore, we need to take into consideration that H_3PO_4 can also work as a stabilizer to suppress the disproportionation of H_2O_2 when reacting with trace levels of metal cations [20] and the resulting decomposition [21]. The mixture with H_3PO_4 can suppress the H_2O_2 reduction resulting in the promotion of H^+. Furthermore, Shiraishi et al. applying Raman spectroscopy and cyclic voltammetry, suggested that H_3PO_4 suppresses the reduction of H_2O_2 by a stronger interaction between H_3PO_4 and H_2O_2 compared with water due to the H-bonding interaction to form an H_2O_2-H_2PO_4- bidentate complex [22]. The authors also advocated that H_3PO_4 associates with H_2O_2 via H-bonding to form a stabilized complex, which may inhibit the H_2O_2 reduction and decrease the enthalpy required to conduct an exothermic reaction, as observed here, thus far proposing that H_3PO_4 is safer and more manageable than H_2SO_4.

Medical implant contamination is a paramount concern that negatively compromises the biomaterials' "gold success": achieving complete clinical healing and restoration [23], thus highlighting that nanotextured surfaces are an important and acceptable strategy to reduce microbial adhesion. Our results suggested that smaller NPs (NP7) could avoid the *S. aureus* adhesion for each growing phase (Figure 3). Interestingly, similar outcomes of bacterial colonization were detected for the NP14, NP36, and control. Moreover, we can focalize that SEM micrographs illustrated an analogous spherical phenotype commonly observed for coccus bacteria (Figure 3, insets). Furthermore, the micrographs suggest that higher biofilm colonization agrees

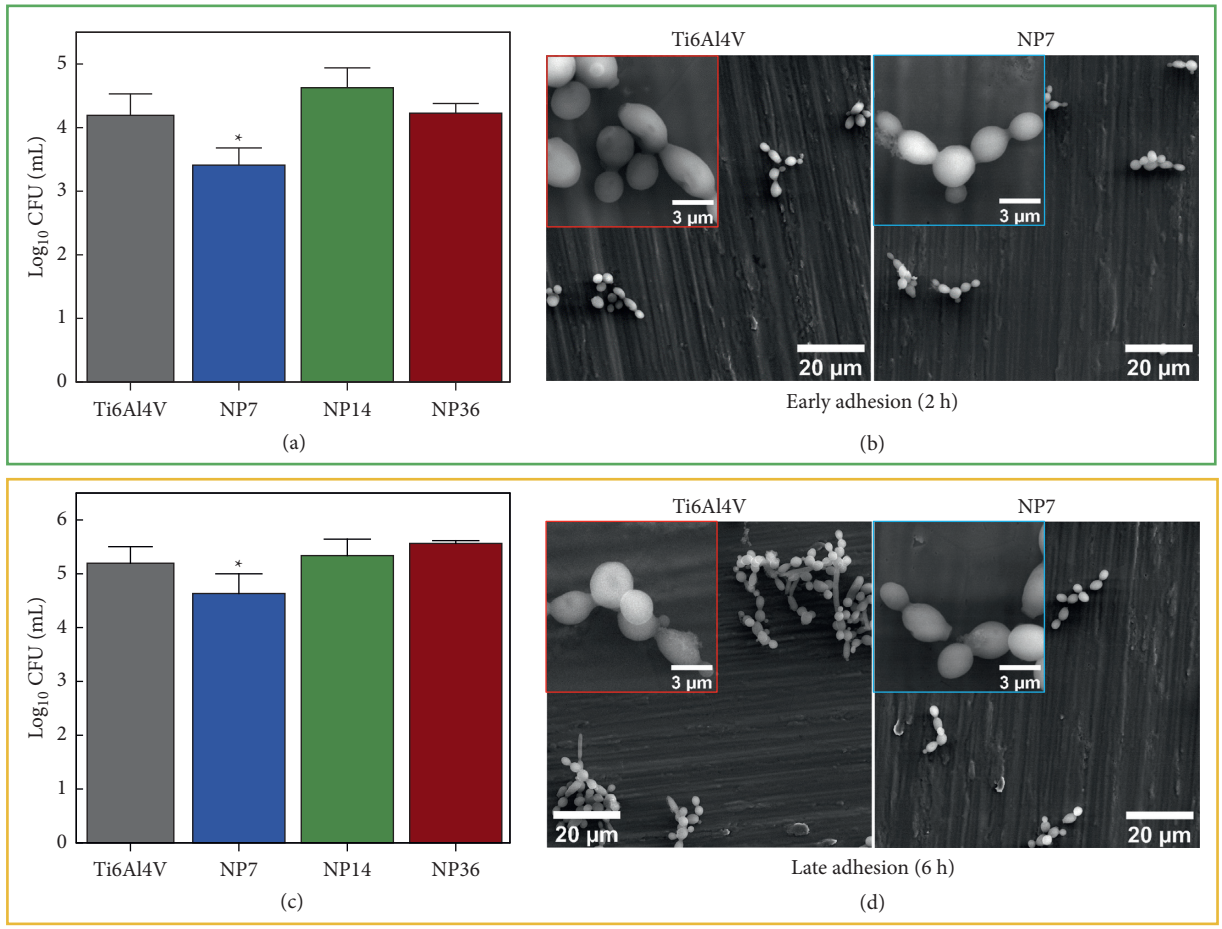

Figure 5: Antifungal analysis on the materials specimens. (a) *C. albicans* viability behavior after 2 h of growth. (b) Fungal morphology characterization on the control and NP7 surfaces at early adhesion phase. (c) *C. albicans* viability counts after 6 h of incubation. (d) Fungal phenotype evaluation at the late adhesion stage. The symbol * illustrates significant differences among the experimental groups.

with the increased viability detected. A similar behavior was detected for the *E. coli* model evaluated on the experimental materials (Figure 4). The *E. coli* growing ability was reduced on the NP7 material in comparison with the study surfaces. Of particular interest is the fact of similar bacterial morphology conducted by the Ti6Al4V alloy and the NP7. The high-zoom micrographs (Figure 4, insets) clearly show that bacilli configuration is present in plenty on the evaluated surfaces. However, from the low-zoom micrographs, we can highlight that the NP7 reduced the bacterial adhesion, as mainly detected at the late adhesion phase. Importantly, the NP7 supported antifungal behavior (Figure 5), following comparable results to those of *S. aureus* and *E. coli*. In the early adhesion, we detected that the control caused enlarged cell alterations, which were further transformed into hyphae and pseudohyphae morphologies. Meanwhile, NP7 conserved a downregulated proliferating phenotype. Principally, we discovered a substantially growing fungal viability for the larger NPs, further proposing that smaller NPs can present detrimental fungal outcomes, as previously reported [24]. Notably, these results suggest that the smaller NPs could disrupt the formation of nanoscale bonds required to conduct a proper microbial adhesion, in accordance with previous works [9, 25]. In particular, the significant hydrophilicity on NP7 may positively influence the reduced electrostatic interactions for microbial bonding [26] and the amorphous nature of the TiO_2 thin coating [27]. However, we recommend more physicochemical studies to explain the current antimicrobial results.

It is well known that the modification of a conventional surface material to its nanostructured counterpart can alter the cellular activity [2, 28, 29]; a critical result presented from this work is the finding that nanoporous surfaces developed by etching with an H_3PO_4/H_2O_2 mixture can improve osteoblast activity. In Figure 6, it is presented the osteoblast viability on the experimental materials after 24 h of culture. The results suggested that the NP7 and NP36 nanostructured surfaces promoted higher cellular proliferation in contrast to the control alloy and the NP14. It is essential to consider that MTT assays take advantage of mitochondrial activity, pointing toward the fact that a higher quantification of resulting formazan crystals is directly proportional to a healthy and active osteoblast growing population [30, 31]. Therefore, we can hypothesize that nanoporous distribution may play a more critical role in promoting early osteoblast proliferation instead of the NP size. This information can be in part supported by the fact that NP7 and NP36 share a more distributed porous size than NP14. On the other hand, NP7

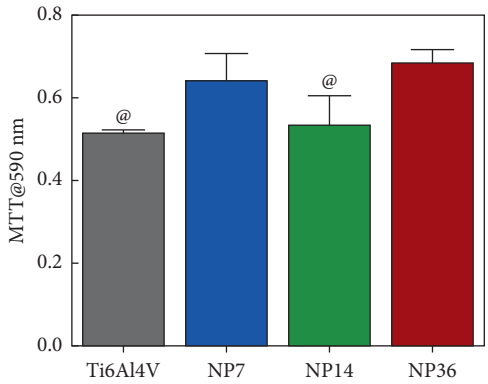

Figure 6: Osteoblast viability assessment after 24 h on the experimental materials. The symbol @ indicates statistical differences against NP7 and NP36.

showed higher osteoblast activity and more hydrophilicity, indicating improved surface energy and enhanced early cellular growth. This current trend opens the concept that a high surface-area-to-volume ratio and improved surface energy can establish a stimulating microenvironment that can accelerate the bone-growing functionality, as depicted in previous studies of different size-controlled nanostructured coatings [32–35].

4. Conclusions

Our results established an oxidative nanopatterning protocol using H_3PO_4/H_2O_2 as a feasible, safer, and controllable system for developing homogeneous nanotextured surfaces on Ti6Al4V. The H_3PO_4/H_2O_2 resulted in a stable mixture that did not show violent exothermic reactions during the preparation of the solutions and the alloy surface modification. Inherently, our protocol resulted in NPs of 7, 14, and 36 nm outlining the reaction time as the main variable for diameter control under the studied synthetic conditions. Importantly, we have demonstrated that smaller NPs can reduce the early adhesion of *S. aureus*, *E. coli*, and more strikingly, *C. albicans*. Thus, more attractively, NP7 tailored a long-lasting antimicrobial action for 6 h of incubation, particularly with the absence of cellular phenotype alterations. On the other hand, the cytotoxicity analysis suggested that the surfaces might not disrupt the initial osteoblasts' proliferation, tailoring the nanostructures as a stable surface for osteoactive conditions. Our work opens a new path for the rationale design of nanobiomaterials with "intelligent surfaces" capable of decreasing microbial adhesion and being scalable for industrial transfer.

Data Availability

All data generated or analyzed in this study are included in this work.

Conflicts of Interest

The authors declare that they have no conflicts of interest.

Authors' Contributions

EBP and BVS contributed to conceptualization, funding acquisition, writing of the original draft, review, and editing.

Acknowledgments

This study was supported by SEP-CONACYT (no. A1-S-38368) and "Proyecto Apoyado por el Fondo Sectorial de Investigación para la Educación" (CB2017-2018).

References

[1] F. Variola, J.-H. Yi, L. Richert, J. D. Wuest, F. Rosei, and A. Nanci, "Tailoring the surface properties of Ti6Al4V by controlled chemical oxidation," *Biomaterials*, vol. 29, no. 10, pp. 1285–1298, 2008.

[2] R. Rasouli, A. Barhoum, and H. Uludag, "A review of nanostructured surfaces and materials for dental implants: surface coating, patterning and functionalization for improved performance," *Biomaterials Science*, vol. 6, no. 6, pp. 1312–1338, 2018.

[3] G. Wang, D. Weng, C. Chen, L. Chen, and J. Wang, "Influence of TiO2 nanostructure size and surface modification on surface wettability and bacterial adhesion," *Colloid and Interface Science Communications*, vol. 34, Article ID 100220, 2020.

[4] F. Variola, S. Francis-Zalzal, A. Leduc, J. Barbeau, and A. Nanci, "Oxidative nanopatterning of titanium generates mesoporous surfaces with antimicrobial properties," *International Journal of Nanomedicine*, vol. 9, p. 2319, 2014.

[5] F. Vetrone, F. Variola, P. Tambasco de Oliveira et al., "Nanoscale oxidative patterning of metallic surfaces to modulate cell activity and fate," *Nano Letters*, vol. 9, no. 2, pp. 659–665, 2009.

[6] D. S. Carretero, C.-p. Huang, J.-H. Tzeng, and C.-p. Huang, "The recovery of sulfuric acid from spent piranha solution over a dimensionally stable anode (DSA) Ti-RuO2 electrode," *Journal of Hazardous Materials*, vol. 406, Article ID 124658, 2021.

[7] Y. Alexeev, T. L. Windus, C.-G. Zhan, and D. A. Dixon, "Accurate heats of formation and acidities for H3PO4, H2SO4, and H2CO3 from ab initio electronic structure calculations," *International Journal of Quantum Chemistry*, vol. 102, no. 5, pp. 775–784, 2005.

[8] P. Kumar, K. Dutta, and P. P. Kundu, "Enhanced performance of direct methanol fuel cells: a study on the combined effect of various supporting electrolytes, flow channel designs and operating temperatures," *International Journal of Energy Research*, vol. 38, no. 1, pp. 41–50, 2014.

[9] E. Beltrán-Partida, B. Valdez-Salas, M. Curiel-Álvarez, S. Castillo-Uribe, A. Escamilla, and N. Nedev, "Enhanced antifungal activity by disinfected titanium dioxide nanotubes via reduced nano-adhesion bonds," *Materials Science and Engineering: C*, vol. 76, p. 59, 2017.

[10] E. Beltrán-Partida, B. Valdez-Salas, A. Escamilla et al., "Disinfection of titanium dioxide nanotubes using superoxidized water decrease bacterial viability without disrupting osteoblast behavior," *Materials Science and Engineering: C*, vol. 60, p. 239, 2016.

[11] B. Valdez-Salas, E. Beltrán-Partida, R. Zlatev et al., "Structure-activity relationship of diameter controlled Ag@Cu nanoparticles in broad-spectrum antibacterial mechanism,"

Materials Science and Engineering: C, vol. 119, Article ID 111501, 2021.

[12] T. Hryniewicz, K. Rokosz, and H. R. Z. Sandim, "SEM/EDX and XPS studies of niobium after electropolishing," *Applied Surface Science*, vol. 263, pp. 357–361, 2012.

[13] Y. Ando, H. Miyamoto, I. Noda et al., "Calcium phosphate coating containing silver shows high antibacterial activity and low cytotoxicity and inhibits bacterial adhesion," *Materials Science and Engineering: C*, vol. 30, no. 1, pp. 175–180, 2010.

[14] B. Cai, N. Jiang, P. Tan et al., "The custom making of hierarchical micro/nanoscaled titanium phosphate coatings and their formation mechanism analysis," *RSC Advances*, vol. 9, no. 70, pp. 41311–41318, 2019.

[15] M. Yada, Y. Inoue, A. Sakamoto, T. Torikai, and T. Watari, "Synthesis and controllable wettability of micro- and nanostructured titanium phosphate thin films formed on titanium plates," *ACS Applied Materials & Interfaces*, vol. 6, no. 10, pp. 7695–7704, 2014.

[16] M. Pisarek, A. Roguska, M. Andrzejczuk et al., "Effect of two-step functionalization of Ti by chemical processes on protein adsorption," *Applied Surface Science*, vol. 257, no. 19, pp. 8196–8204, 2011.

[17] V. Likodimos, T. Stergiopoulos, P. Falaras, J. Kunze, and P. Schmuki, "Phase composition, size, orientation, and antenna effects of self-assembled anodized titania nanotube Arrays: a polarized micro-Raman investigation," *Journal of Physical Chemistry C*, vol. 112, no. 33, pp. 12687–12696, 2008.

[18] P. Kern, C. Jäggi, I. Utke, V. Friedli, and J. Michler, "Local electron beam induced reduction and crystallization of amorphous titania films," *Applied Physics Letters*, vol. 89, no. 2, Article ID 021902, 2006.

[19] C. Sittig, M. Textor, N. D. Spencer, M. Wieland, and P. H. Vallotton, "Surface characterization of implant materials c.p. Ti, Ti-6Al-7Nb and Ti-6Al-4V with different pretreatments," *Journal of Materials Science. Materials in Medicine*, vol. 10, pp. 35–46, 1999.

[20] N.-H. Kim, J.-H. Lim, S.-Y. Kim, and E.-G. Chang, "Effects of phosphoric acid stabilizer on copper and tantalum nitride CMP," *Materials Letters*, vol. 57, no. 29, pp. 4601–4604, 2003.

[21] W. C. Schumb, "Stability of concentrated hydrogen peroxide solutions," *Industrial and Engineering Chemistry*, vol. 41, no. 5, pp. 992–1003, 1949.

[22] Y. Shiraishi, Y. Ueda, A. Soramoto, S. Hinokuma, and T. Hirai, "Photocatalytic hydrogen peroxide splitting on metal-free powders assisted by phosphoric acid as a stabilizer," *Nature Communications*, vol. 11, no. 1, p. 3386, 2020.

[23] Y. F. Cheng, Y. H. Mei, G. Sathishkumar et al., "Tannic acid-assisted deposition of silk sericin on the titanium surfaces for antifouling application," *Colloid and Interface Science Communications*, vol. 35, Article ID 100241, 2020.

[24] B. Valdez-Salas, E. Beltrán-Partida, N. Nedev et al., "Controlled antifungal behavior on Ti6Al4V nanostructured by chemical nanopatterning," *Materials Science and Engineering: C*, vol. 96, pp. 677–683, 2019.

[25] C. Lüdecke, M. Roth, W. Yu, U. Horn, J. Bossert, and K. D. Jandt, "Nanorough titanium surfaces reduce adhesion of *Escherichia coli* and *Staphylococcus aureus* via nano adhesion points," *Colloids and Surfaces. B, Biointerfaces*, vol. 145, pp. 617–625, 2016.

[26] L. Zheng, S. Qian, and X. Liu, "Enhanced osteogenic activity and bacteriostatic effect of TiO2 coatings via hydrogen ion implantation," *Materials Letters*, vol. 253, pp. 95–98, 2019.

[27] B. Valdez-Salas, E. Beltrán-Partida, M. Curiel-Álvarez, M. Guerra-Balcázar, and N. Arjona, "Crystallographic pattern mediates fungal nanoadhesion bond formation on titanium nanotubes," *ACS Omega*, vol. 6, no. 24, pp. 15625–15636, 2021.

[28] E. Beltrán-Partida, A. Moreno-Ulloa, B. Valdez-Salas et al., "Improved osteoblast and chondrocyte adhesion and viability by surface-modified Ti6Al4V alloy with anodized TiO2 nanotubes using a super-oxidative solution," *Materials*, vol. 8, p. 867, 2015.

[29] J. C. M. Souza, M. B. Sordi, M. Kanazawa et al., "Nano-scale modification of titanium implant surfaces to enhance osseointegration," *Acta Biomaterialia*, vol. 94, pp. 112–131, 2019.

[30] A. M. Beyer, L. E. Norwood Toro, W. E. Hughes et al., "Autophagy, TERT, and mitochondrial dysfunction in hyperoxia," *American Journal of Physiology - Heart and Circulatory Physiology*, vol. 321, no. 5, pp. H985–H1003, 2021.

[31] N. Duewelhenke, O. Krut, and P. Eysel, "Influence on mitochondria and cytotoxicity of different antibiotics administered in high concentrations on primary human osteoblasts and cell lines," *Antimicrobial Agents and Chemotherapy*, vol. 51, no. 1, pp. 54–63, 2007.

[32] K. Gulati, H.-J. Moon, T. Li, P. T. Sudheesh Kumar, and S. Ivanovski, "Titania nanopores with dual micro-/nano-topography for selective cellular bioactivity," *Materials Science and Engineering: C*, vol. 91, pp. 624–630, 2018.

[33] R. Aguirre Ocampo, M. Echeverry-Rendón, S. Robledo, and F. Echeverría Echeverría, "Effect of TiO2 nanotubes size, heat treatment, and UV irradiation on osteoblast behavior," *Materials Chemistry and Physics*, vol. 275, Article ID 125137, 2022.

[34] K. S. Brammer, S. Oh, C. J. Cobb, L. M. Bjursten, H. v. d. Heyde, and S. Jin, "Improved bone-forming functionality on diameter-controlled TiO2 nanotube surface," *Acta Biomaterialia*, vol. 5, no. 8, pp. 3215–3223, 2009.

[35] C. Mas-Moruno, B. Su, and M. J. Dalby, "Multifunctional coatings and nanotopographies: toward cell instructive and antibacterial implants," *Advanced Healthcare Materials*, vol. 8, no. 1, Article ID 1801103, 2019.